Around the corner: Colloidal assembly and wiring in groovy nematic cells

Yimin Luo, Francesca Serra, Daniel A. Beller, Mohamed A. Gharbi, Ningwei Li, Shu Yang, Randall D. Kamien, and Kathleen J. Stebe

Phys. Rev. E **93**, 032705 — Published 25 March 2016

DOI: 10.1103/PhysRevE.93.032705

Around the corner: colloidal assembly and wiring in groovy nematic cells

Yimin Luo,[1] Francesca Serra,[1] Daniel A. Beller,[1,2] Mohamed A. Gharbi,[1,3]
Ningwei Li,[1] Shu Yang,[1] Randall D. Kamien,[1] and Kathleen J. Stebe[1,*]

[1] *Laboratory for Research on the Structure of Matter (LRSM), University of Pennsylvania, Philadelphia PA*
[2] *School of Engineering and Applied Sciences, Harvard University, Cambridge, MA*
[3] *Department of Physics, McGill University, Montreal, Quebec, Canada*

We study colloids suspended in nematic liquid crystal in grooves with homeotropic anchoring. We observe "eyelashes", topological dipole chains that follow the local, curved director field. These beget wires that connect the groove corners to topographical features on the cell lid to yield oriented, curvilinear colloidal wires spanning the cell, formed in a non-singular director field. As the groove aspect ratio changes, we find different ground states and corroborate our observation with numerics. Our results rely upon on the scale of topographical features, the sharpness of edges, and the colloid-sourced distortions; all these elements can be exploited to guide the formation of reconfigurable structures in nematics.

I. INTRODUCTION

Colloidal inclusions in liquid crystals (LCs) provide a way to connect the visible to the invisible. By observing the interactions and assembly of the micron-scale colloids we can deduce the nature of the nanoscale, anisotropic liquid crystals [1–3], just as large colloids can reveal the size and organization of small colloids in isotropic systems [4]. Topology, through boundary conditions, controls the foundation of this interaction: particles not only distort the LC field but also change the structure of the boundary. For example, a colloidal particle that imposes perpendicular (homeotropic) anchoring of the LC molecules in a container with incompatible boundary conditions requires the introduction of an excess topological charge that forces defects into the sample [5]. Together with the colloid, these "companion defects" create localized distortions with dipole and quadrupole character [6] (Fig. 1(a,b)). At long distances, the nonlinear elasticity is well approximated by a linearized theory and these multipoles interact as standard linear dipoles and quadrupoles in bulk. Dipoles form straight strings of colloids aligned with the director field (Fig. 1(c)), while quadrupoles, aligning perpendicular to the field, generate either a zig-zag string (Fig. 1(d)) or a straight line at an oblique angle with respect to the director field [7–9]. At the same time, colloids can act as impurities and be attracted to defect lines (disclinations) in the bulk, an effect that has been used to create wires of colloids spanning a cell from top to bottom [10–12]. Since disclinations can be attached to precise locations by controlling the boundary conditions, they can collect colloids and be stabilized by them in turn [13]. But are disclination lines necessary to create colloidal wires of nontrivial geometry? In this paper, we demonstrate the self-assembly of topological dipoles into controllable, oriented, curvilinear colloidal wires in a non-singular director field, without disclination lines.

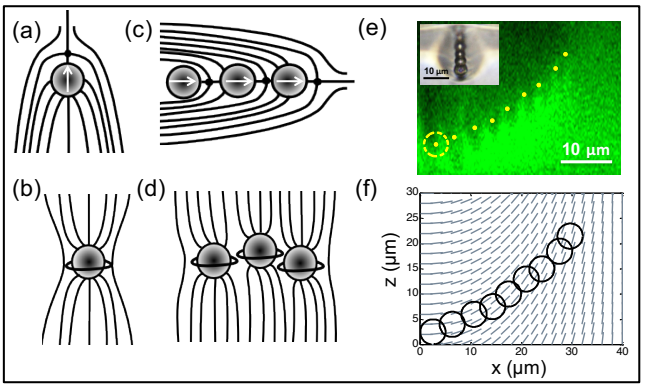

FIG. 1. Director field around colloids with homeotropic anchoring and their curvilinear assembly. Topological (a) dipoles and (b) quadrupoles. Assembly of (c) dipoles (straight) and (d) quadrupoles (zigzag) in NLC. (e) An "eyelash": a curvilinear string of colloids as reconstructed from confocal microscopy. A dashed circle indicates the position of the first colloid and dots indicate the center of the mass of successive colloids in the chain. Inset: top view of the eyelash under bright field (BF). (f) Position of the colloids in (e) forming an eyelash (circles), superimposed on the director field approximated with a 2D escape in $\hat{z}$: $\theta = 2\arctan(\frac{x}{x_0})$, where θ is the angle between the director and the vertical direction and $x_0 = 40\mu$m [14].

We confine nematic liquid crystal (NLC) in rectangular grooves with corners that act as strong attraction sites for colloids. In large, shallow grooves, disclination lines are absent, the director field is non-singular and corners act as docking sites. Upon docking, each colloid-defect topological dipole attracts more colloids in bulk to form roughly equispaced curvilinear "eyelashes" that start at interior corners and follow the director field. One such eyelash is shown in Fig. 1(e): a chain of dipoles assembles in a curvilinear fashion, following the director field (Fig. 1(f)). Our demonstration that the local dipole field can be persuaded to follow a curvilinear director field offers a new modality for templating complex and variegated structures in colloid/liquid crystal systems. In-

* kstebe@seas.upenn.edu

trigued by the complementary findings of Galerne and co-workers [10, 11], who formed cell-spanning colloidal wires on disclination lines seeded to begin and end at anchoring cues, here we seek to form cell-spanning wires along director field lines by placing the right topographical cues at the top and bottom surfaces to shape the smooth director field – the colloidal dipoles will follow. Finally, we show that this assembly mode is only possible for a certain range of aspect ratios of the grooves. For thinner grooves, the particles assemble along defect lines.

II. EXPERIMENTAL

A. Sample preparation

We suspended silica particles (Polysciences, Inc., 0.1 wt%) with 5μm diameter and strong homeotropic anchoring [15] in square grooves filled with 5CB (4-cyano-4'-pentylbiphenyl, Kingston Chemicals, clearing point $T_{NI} \approx 34.9$°C). The grooves, fabricated using soft lithography of epoxy resin SU8 (MicroChem Corp.) [16], were sputtered with chrome, treated with a solution of 3wt% DMOAP (dimethyloctadecyl[3-(trimethoxysilyl)propyl], Sigma-Aldrich) in de-ionized (DI)-water and annealed at 80°C, to achieve strong homeotropic anchoring, following the procedure in [15]. The glass lid placed on top of the grooves was also treated with a 3wt% DMOAP solution in DI water. The total thickness of the cell was controlled by a Mylar spacer to locate the lid 10-20μm above the grooves, as shown in Fig. 2(a). For some experiments, we added additional features to the top glass to guide the assembly: an SU8 square pillar array (height $h = 5\mu$m, sides $s = 5\mu$m, pitch $p = 50\mu$m) to the top cover slip. The surface of the SU8 pillar array was coated with silica, through chemical vapor deposition of silicon tetrachloride ($SiCl_4$, Sigma-Aldrich) and functionalized with DMOAP. The colloidal suspension in liquid crystals was vortexed for 15 minutes before the filling to break up aggregates. The channels were filled along the direction of the grooves by capillary actions in isotropic phase. Then the cell was allowed to cool below the clearing point.

B. Imaging

The channels ware imaged by an upright microscope (Zeiss AxioImager M1m) in the transmission mode equipped with crossed polarizers. The images were captured by high-resolution camera (Zeiss AxioCam HRc). Objectives' magnification ranged from 20x to 100x. To determine the director field orientation, fluorescence confocal polarizing microscopy (FCPM) was performed, following the method in [17], with an inverted IX81 Olympus microscope equipped with a half-wave plate between the objective and filter cubes which serves to change the polarization of the scanning laser. While FCPM is useful to characterize LC director fields in many settings, in this particular case one has to take into account optical aberrations that can neither be ignored, nor avoided. Additional details can be found in Appendix A.

C. Particle tracking

The dynamic process of assembly was explored in a set of channels (height $h = 50\mu$m, width $w = 300\mu$m) through video tracking over the course of about 5 hours. After this time, most of the colloids had migrated away from the middle of the channel, indicating the long-range influence of the corner, which permeates the entire channel width ($\frac{w}{2} = 150\mu$m). The video was taken under cross-polarizers at the rate of one image every 30 seconds (Video 2, SM, speed×1800), and post-processed using the ImageJ-based software FIJI to extract the 2D trajectories of the particles. For simplification, aggregates of particles were excluded from the tracking analysis.

III. RESULTS AND DISCUSSION

A. Wide grooves

In wide grooves ($w = 100\mu$m and $h = 50\mu$m), the colloids self-assemble into eyelashes that follow the director field. An eyelash is shown in Video 1 [18], in images captured by moving the objective focus. A top view of the cell is presented in Fig. 2(b) under polarized optical microscopy (POM), which shows evenly spaced eyelashes along the length of the groove. We deduced the director field with the aid of POM, FCPM (Fig. 2(c)), and via simulation using a Q-tensor based Landau-de Gennes (LdG) model following [19–21] (Appendix B). The director field starts perpendicular to the walls and then bends upwards creating a middle region where it is completely aligned along $\hat{z}$, as sketched in Fig. 2(d). This configuration was observed in other LC/colloidal systems with similar geometries [15, 22, 23].

We observe that colloids are attracted to the interior corners (marked 2 and 3 in Fig. 2(d)) between the groove walls and the bottom substrate. These are the regions of strongest splay distortion, where the radius of curvature is small ($\approx 3\mu$m based on scanning electron microscopy measurements). The matching length scale and anchoring conditions between the particle and the corners favors the attraction of the particles, despite the fact that a flat wall with the same anchoring condition would show a repulsive interaction. Although this resembles qualitatively the so-called "key-lock" mechanism [24, 25], the two mechanisms do not precisely coincide: the former has been discussed in the context of particles surrounded by a "Saturn ring", a topological quadrupole [6, 26, 27], while here each particle has an associated hyperbolic point defect, making a topological dipole [7, 28]. However, the mechanisms are indeed related: colloids are attracted to docking sites to minimize the distortion of the director

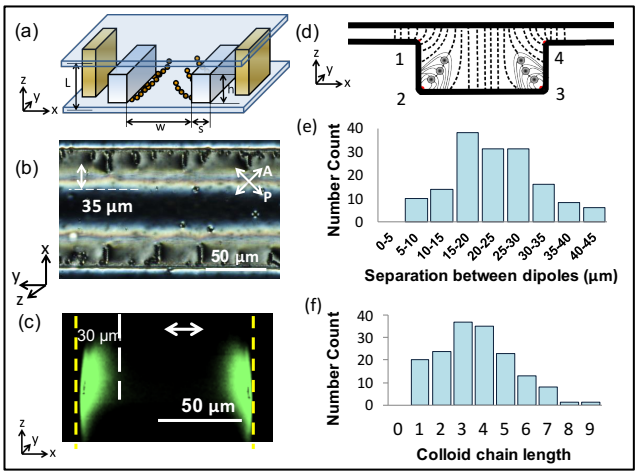

FIG. 2. Curvilinear assembly forming eyelashes and wires in confined cells. (a) Schematic of cell geometry. (b) POM image of the top view of a channel ($h = 50\mu$m, $w = 100\mu$m). Chains are periodically spaced ($\approx 15-20\mu$m) along the bottom edge of the channel. (c) FCPM of a colloid-free channel of the said dimension. The laser is polarized along $\hat{x}$. (d) Schematic of director field in the groove with the dipolar chains (confirmed by simulation). Histograms of (e) colloidal chain lengths and (f) separations between neighboring dipoles. Only chains that are part of a cluster of 10 or more chains are considered for statistical purposes.

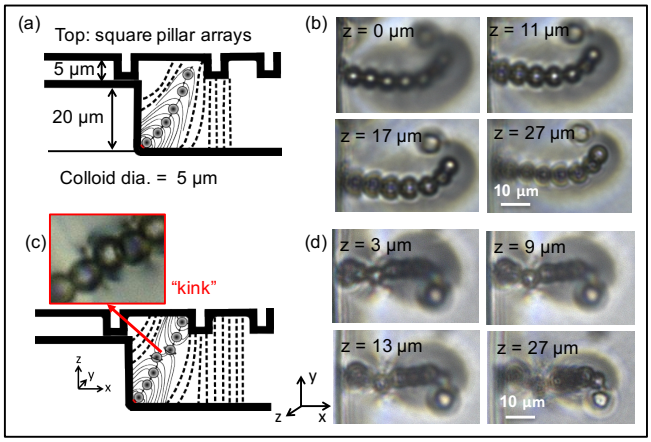

FIG. 3. Cell-spanning wires created by imposing topographical cues. (a) Schematics of an incomplete wire. (b) BF images with z positions focusing on various points on the wire. The dipole approaches the feature on the top but stops at an equilibrium distance. The chain bends towards the pillar. (c) Schematic and (d) images at different focal planes of a complete wire, formed by reconciling two opposing chains of dipoles with quadrupoles. Inset: experimental observation of a "kink" of connected Saturn rings.

field. When the first colloid attaches to the bottom corner, its associated defect points outwards towards the center of the channel. The orientation of the topological dipole propagates along the dipolar chain, which is also outward-pointing (Fig. 2(d)). Thus, typically, the eyelashes are chains of dipoles, starting at the bottom corner of the grooves and following the bending of the director field. The uniform spacing of the eyelashes (≈15-20 μm, Fig. 2(b) and 2(e)), can be attributed to repulsion between the oriented dipolar chains [29]. As dipolar repulsion dictates the spacing between neighboring eyelashes, the polydispersity in spacing between the chains mirrors the polydispersity in the chain lengths (Fig. 2(f)).

These assemblies might be exploited, for example, as micro-cilia or micro-mixers. However, many more applications would be possible if we were able not only to *start* and *direct* the wires, but also to *terminate* them and *connect* them between two surfaces: they could template conductive wires or act as soft corrals.

B. Chains of particles

To create such connected chains of particles, we added a square pillar array (height $h = 5\mu$m, sides $s = 5\mu$m, pitch $p = 50\mu$m) to the top cover slip, treated to have homeotropic anchoring, like "stalactites", which may provide a second topographical anchor.

We observe dipolar chains that start at the bottom corner of the groove and follow the director field that bends towards the inverted pillar (Fig. 3(a)). However, a problem emerges at the end of the chain: all the point defects in the chain point outwards, including the last one; the mismatch of dipole orientation prevents the end colloid from attaching to the interior corner at the bottom of the pillar. Instead, the dipolar chain stops at an equilibrium distance from the pillar (Fig. 3(a,b)). A similar scenario takes place when a chain attaches to the pillar first and follows the director field and reaches for the bottom of the channel. The attraction to corners relies upon a particular polarity that propagates along the chain – is wiring still possible?

The interior corners of the pillars on the top lid can also act as cues to initiate a colloidal chain. Two chains extending from the base of the pillar and the bottom of the groove, respectively, can be guided into close proximity by the director field. When the two dipolar chains are close enough, they have mismatched orientations that frustrate the formation of a wire. However, we observe a restructuring of the defects – the terminal colloids of the two chains become quadrupoles. The partner point defect opens up into a ring that then hugs the colloid, seamlessly connecting two antagonistic chains of dipoles while conserving the topological charge. By eliminating the dipolarity the chains can join in the zig-zag configuration (Fig. 3(c,d)), creating a cell-spanning chain (shown in Video 2 in [30]).

C. Particle-corner interaction

We have demonstrated that dipole orientation plays a key role in the formation of the eyelash chains. How do colloids behave far from the corners? We tracked seven sets of 2D trajectories in bulk using optical video microscopy (Fig. 4(a,b)); the trajectories are decomposed in $\hat{x}$, perpendicular to the groove axis, and $\hat{y}$, parallel to it (Video 3 in [31]). Migration in $\hat{z}$ is small compared to $\hat{x}$ ($\approx 150\mu$m), the reason being that the center of mass of a 5μm colloid levitates 12μm from the bottom wall [32]. We observe that the movement is (roughly) Brownian in $\hat{y}$ (Fig. 4(c)), while ballistic in $\hat{x}$ (Fig. 4(b,d)). We plot the distance $|x - x_f|$ versus time until contact $t_f - t$ (Fig. 4(b)), where x_f and t_f are the final (equilibrium) position and time. To infer the interaction potential U between the particle and the corner, we note that the particle migrates in creeping flow, *i.e.* with Reynolds number $Re = \frac{\rho v l_c}{\mu} = 6.9 \times 10^{-8} \ll 1$ and non-Newtonian effects are negligible, *i.e.* the Erickson number $Er = \frac{\mu v l_c}{K} = 0.03 \ll 1$ based on typical values for the material parameters in literature [33]. Thus, the interaction force $F_{elastic} = -dU/dx$ is balanced by the drag force on the isolated particle $F_{drag} = 6\pi\eta r \frac{dx}{dt}$. We fit the trajectories by truncating them at a distance $d > 70\mu$m to ensure a small director gradient and to avoid hydrodynamic interactions with the boundary, and find $|x - x_f| \sim (t_f - t)^{\frac{1}{5}}$. From this power law, we infer that $F_{elastic} \sim 3Ax^{-4}$, and that the particle is attracted toward the corner with a potential $U \sim -Ax^{-3}$, (Fig. 4(d)) compatible with the physical picture of a dipole-dipole interaction.

We think of this interaction this way: the corner creates a spatially varying host director field with gradients that are steep in the vicinity of the corner and then weaken far from it (Fig. 5(a)). When the gradients are sufficiently weak, the host field can be expressed in a multipole expansion around any position. A particle at that position perturbs the field, both via the colloid-associated defect and via an induced mode, both of dipolar form, that decay with distance from the particle. These terms interact, yielding the observed potential U. In the steep slope region (Fig. 5(b)), the assumption of weak gradients in the director field no longer applies and the interaction no longer has such a simple form. Rather, we think of this near field interaction as being akin to the lock-and-key mechanism. By nestling in the corner, the colloid removes regions of steep gradients. The particle distortion is well accommodated by the distortion near the wall due to the anchoring conditions of particle and wall. Thus the corner favors the nestling of the particle near the corner, as the liquid crystal can be well oriented in the interstitial region between the particle and the corner.

Far from the corners, colloids experience a weak interaction and migrate very slowly. During this lag-time, they may also interact with other colloids forming free-floating, short chains in bulk (Fig. 6 shows a pair of colloids merging onto an eyelash). These relatively rigid chains migrate to the end of the chain and alter the overall shape of the eyelash. This suggests that the use of narrower grooves would prevent these unwanted aggregates. Furthermore, it would speed up the assembly of both eyelashes and wires (*e.g.* total time of assembly goes from thousands of seconds for channel width $w = 300\mu$m to tens of seconds for $w = 75\mu$m). We pursued this task and found that, indeed, narrower grooves do speed up assembly, up to a point. However, strong distortions in very narrow grooves spoil the mechanism.

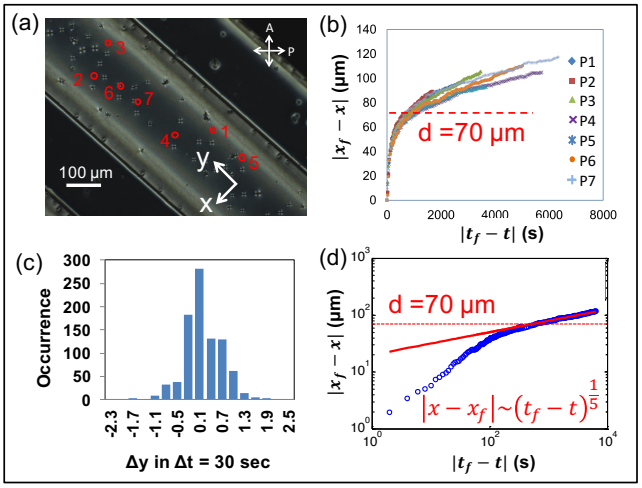

FIG. 4. Dynamics of assembly for eyelashes. (a) Positions of the colloids tracked in Video 2 (SI), under POM, decomposed in $\hat{x}$ and $\hat{y}$. (b) $\hat{x}$-trajectories are ballistic and overlap with each other. The dotted line denotes location of $d = 70\mu$m away from the wall. (c) Displacement distribution Δy in $\hat{y}$ (roughly Gaussian). (d) The $|x - x_f|$ vs. $t_f - t$ plot, fit with a dipolar potential (red solid line) only in the far field (above the red dashed line).

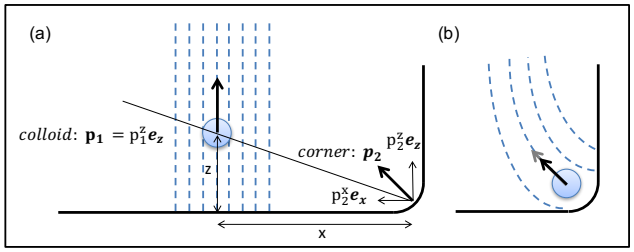

FIG. 5. Schematic of the colloid(1)-corner(2) dipole-dipole interaction in (a) far-field and (b) near-field.

D. Narrow grooves

In narrow grooves, we observe one or more colloid-decorated defect lines, as shown in Fig. 7(a,b). The changes in colloidal assembly correspond to changes in

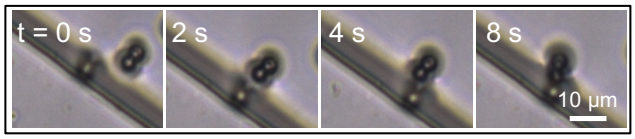

FIG. 6. A pair of colloids approaches the near-field of a dipole that is already anchored at the bottom corner.

the director field: in wide grooves, the director field escapes along $\hat{z}$ via splay-bend deformation. In narrower grooves, the two regions of strong splay distortion near the corners come into such proximity that the original configuration is no longer energetically favorable. In the absence of colloids, this leads to an escape in $\hat{y}$ as shown in Fig. 7(c). However, colloids can lower the free energy cost of defects by inserting themselves into the cores of topological defects [13].

We performed POM, FCPM (Appendix A), and Q-tensor simulations (Appendix B) in grooves with different aspect ratios and find that in narrow grooves one of the bottom corners has a bend configuration instead of a splay configuration. This splay-bend transition in corners resemble that discussed in the context of wetting phenomena in 2D grooves [34, 35]. If a colloid is nested near the corner, then the corner can keep the splay distortion. The bend distortion is accommodated on top of the colloid, where the surface anchoring is violated. The compression of the director field leads to breaking the symmetry of the groove: the other bottom corner, in fact, keeps the usual splay distortion with the associated eyelashes as shown in Fig. 7(d).

In even narrower grooves, the homeotropic side walls require the director field to align along $\hat{x}$. The distortion is confined to the top and bottom of the groove. In this configuration, the cell is effectively segregated into two "half cells," each with hybrid boundary conditions (Fig. 7(e)). This director field is consistent with simulation, and was observed in FCPM images obtained using low-birefringent nematic LCs to avoid optical artifacts (Fig. 8, Appendix A). The appearance of these defect lines is similar to the case discussed in the context of microfluidic channels [22]: each half cell traps a long defect line that travels along the corners, occasionally crossing the channel in an irregular zig-zag. In this arrangement, "line 1" is pinned at the top edge while "line 2" is located at the bottom, mutually repulsed from each other (see Fig. 7(b,e)). As defect lines form and find their way to either the top or the bottom corner, they collect colloids along the way, creating beads on a chain (Video 4 in [36]). The system breaks the yz-plane reflection symmetry and nucleates one or more defects, rather than escaping along $\hat{y}$, because colloids interact with defects and lower their energetic cost. The simulations predict qualitatively similar results as shown here (Fig. 9 in Appendix B).

These findings suggest that the geometry of the groove

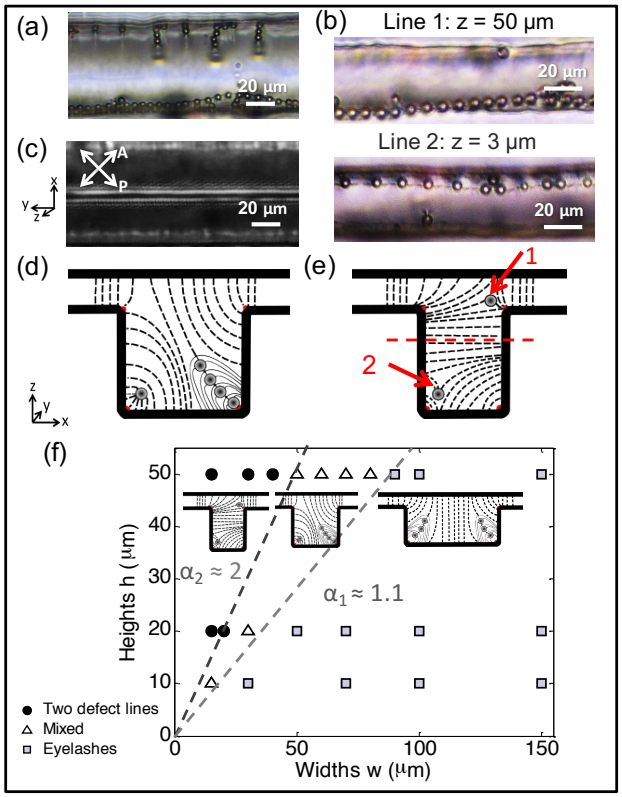

FIG. 7. Transition from eyelashes along director field to strings of colloids along disclination lines. BF images of (a) mixed state with eyelashes and a disclination line that traps colloids ($w = 60\mu$m, $h = 50\mu$m), (b) state which traps two defect lines decorated by colloids ($w = 30\mu$m, $h = 50\mu$m), and (c) POM image of an escape in $\hat{y}$ in a groove with the same dimension as (a) but without colloids. (d-e) Schematics of the director field in (a) and (b) respectively. (f) "Phase diagram" of the structures formed in various geometries. Channel heights h are controlled by spin rates of SU8 photoresist and widths w by photolithography masks.

determines the mode of assembly. In order to quantify this effect, we built a set of grooves with different heights h and widths w to study LCs in structures with different aspect ratio $\alpha = 2h/w$ (Fig. 7(f)). Experimentally, the change in colloidal assembly behavior first occurs at $\alpha_1 \approx 1.1$, where the eyelashes stop growing from both sides and only nucleate from one corner. When $\alpha_2 \approx 2$, our system traps two strings of colloids. For $\alpha_1 < \alpha < \alpha_2$ we observe both morphologies. Our observations are in reasonable agreement with our Q-tensor numerics that predict the onset of yz-plane reflection symmetry-breaking at $\alpha_1 = 1.1$ and the alignment in $\hat{x}$ at $\alpha_2 = 2.9$. The numerically calculated director fields agree qualitatively with experimental observation. We do not argue, however, that the simulation faithfully mirrors the experiments, due to the different lengthscales involved. In simulation, the colloid is so small that it acts as an

impurity; while in experiment one must consider the interaction between the hedgehog and the defect line.

IV. CONCLUSIONS

In conclusion, we have demonstrated two different modes of colloidal assembly in one NLC system. Colloids have "dual-functionalities": as parts of "eyelashes", chains of oriented dipoles following a curved director field, or in the more familiar assembly along disclination lines. The intricate energy landscape near regions of high curvature causes a diverse set of structures to form as the groove geometry is varied. These results rely on the interplay of confinement, edge sharpness, and the distortions induced by the colloids and their associated defects. The eyelashes themselves might be exploited, *e.g.*, as micro-cilia, actuated by flow or by field. By introducing the right topographical cues, they can be manipulated to form full "wires" connecting two walls of a LC cell. This work establishes a new tool to make 3D reconfigurable structures.

ACKNOWLEDGMENTS

We acknowledge discussions with J. Crocker, Z.S. Davidson, N. Engheta, L. Kang, M. Ravnik, A. Sengupta, and N. Sharifi-Mood and experimental assistance from I.B. Liu and Z. Shi. We thank T. Baumgart for access to FCPM. This work was supported in part by NSF MRSEC Grant DMR11-20901. D.A.B. was supported by Harvard University through the George F. Carrier Fellowship, R.D.K. by a Simons Investigator Grant from the Simons Foundation.

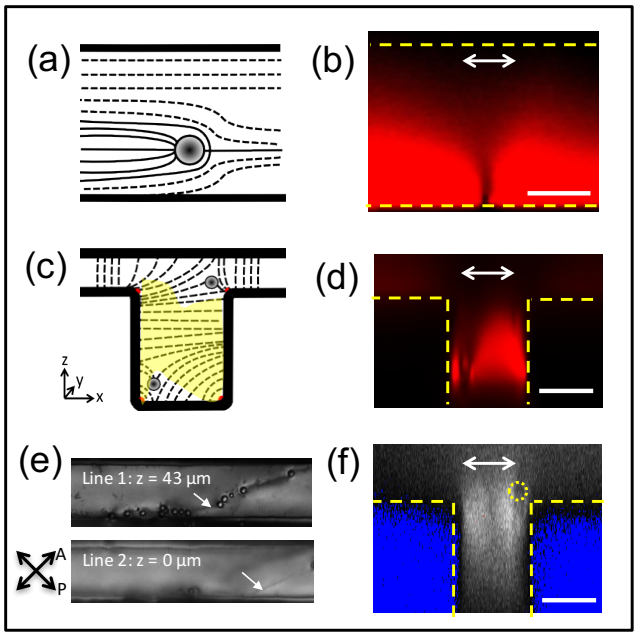

FIG. 8. FCPM measurements with 5CB and CCN mixture. The scale bars are 20μm. Yellow dashed lines denotes boundary of the cell in confocal reconstruction (b)(c)(d). (a) A sketch of the director field of a uniformly-aligned planar cell containing a colloid. (b) FCPM of the cell showing a cone-like shadow above the colloid and extinction of signals at about 20μm above the the colloid. (c) A sketch of the director field of the director configuration inside of a groove with $h = 50\mu$m and $w = 30\mu$m, where regions of alignment in $\hat{x}$ are highlighted, which are expected to give signal. (d) FCPM of the cell in (c) showing similar extinction pattern and conical section in (b). (e) POM images of the two defect lines in the said cell filled with CCN mixture and colloids. (f) FCPM result of the cell in (e) showing alignment in $\hat{x}$, consistent with the prediction in (c). The blue color is due to lack of signal (underexposure) inside the groove.

Appendix A: Fluorescent confocal polarizing microscopy (FCPM)

We performed the experiment with two different LCs: 5CB, which was used in the experimental system, and a binary mixture of low birefringent materials, 4'-butyl-4-heptyl-bicyclohexyl-4-carbonitrile (CCN-47, Nematel GmbH & Co. KG) and 4,4'-dipentyl-bicyclohexyl-4-carbonitrile (CCN-55, Nematel GmbH & Co. KG). This mixture is nematic at room temperature and has low birefringence, and is often adopted as a model system when textures in nematics are characterized using optical methods. The LCs were doped with with 0.01 wt% dye, N,N'-bis(2,5-di-tert-butylphenyl)-3,4,9,10-perylenedicarboximide (BTBP). The dye follows the orientation of the liquid crystal mesogens. It was excited at 534 nm and emits at 585-610 nm [17].

Initial FCPM trials with 5CB suffered from scattering of index-mismatched colloids and high birefringence, even for a uniformly-aligned cell (Fig. 8(a,b)) where the signal right above the colloid is obstructed by a cone-like shadow (Fig. 8(b)), due to scattering off the colloid. This effect can be mitigated to a great extent by using a low birefringence material such as the CCN mixture. However, in the case of 5CB, the lower defect line, Line 2, trapped more colloids, while in the case of CCN mixture, the top one, Line 1, trapped more colloids. The slight difference might be due to the difference in elastic constants of the LCs, which leads to a different levitation force. The difference translated into a different FCPM image (Fig. 8(f)), where the top corner was slightly darker than the bottom due to scattering from the colloids. Nevertheless, Fig. 8(f) showed a bright region and largely horizontal alignment in mid-height of the cell, which was consistent with the prediction of the director field in Fig. 8(c).

Appendix B: Landau-de Gennes Theory and notes on Simulations

The director configurations are corroborated by Landau-de Gennes (LdG) theory-based numerical minimization. We minimize the following free energy functional with respect to the standard Q-tensor:

$$F_{LdG} = \int_{\Omega} dV \left[f_{phase} + f_d \right] \tag{B1}$$

where Ω is the total volume, f_d is the energy density of elastic distortion and

$$f_{phase} = \frac{1}{2} A \operatorname{tr}(Q^2) + \frac{1}{3} B \operatorname{tr}(Q^3) + \frac{1}{4} C \left[\operatorname{tr}(Q^2) \right]^2 \tag{B2}$$

Given for uniaxial nematics,

$$Q = \operatorname{diag}(S, -\frac{1}{2}S, -\frac{1}{2}S) \tag{B3}$$

Therefore,

$$\operatorname{tr}(Q^2) = \frac{3}{2} S^3 \tag{B4}$$

$$\frac{1}{3}\operatorname{tr}(Q^3) = \det(Q) = \frac{1}{4} S^3 \tag{B5}$$

And thus,

$$f_{phase} = \frac{3}{4} A S^2 + \frac{1}{4} B S^3 + \frac{9}{16} C S^4 \tag{B6}$$

In the one constant approximation,

$$f_d = \frac{L}{2} \frac{\partial Q_{ij}}{\partial x_k} \frac{\partial Q_{ij}}{\partial x_k} \tag{B7}$$

We then minimize the LdG free energy over $Q(x)$ with a finite difference scheme on a regular cubic mesh [20], using a conjugate gradient algorithm from the ALGLIB package (www.alglib.net) [19]. The mesh size corresponds to 4.5 nm. The simulation is 222 times smaller than the experimental settings (see additional comment below). An elastic constant $L = 8 \times 10^{-12}$N corresponds to a Frank elastic constant $K \approx 10^{-11}$N. All corners are rounded with a circular arc of radius 9 nm. In the simulations with colloids, the colloids have diameters of $d = 22.5$ nm. The anchoring strength on the surface of the colloids is set to be the same as the wall and equal to 5.82 in the simulation unit, corresponding to a typical anchoring strength of $W_0 = 1 \times 10^{-2} J/m^2$. In simulations without colloids, the wall has infinite anchoring strength. Each simulation is carried out in a thin slice in $\hat{y}$ of thickness = 22.5 nm. The simulation box has the same depth as the colloid diameter (22.5 nm), but is several times larger in length (225 nm) and width (450 nm). With periodic boundary conditions along the y-direction (depth), the simulation is quasi-2D. We have verified that the director field in the simulation does not vary in $\hat{y}$-direction.

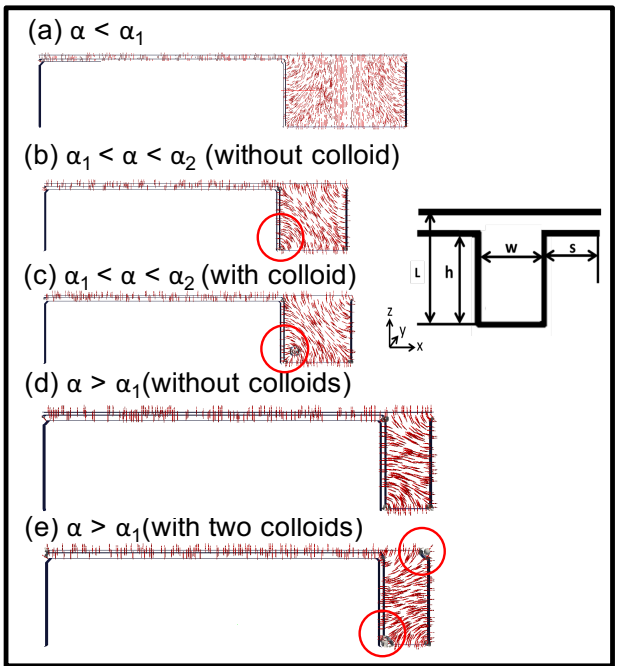

FIG. 9. Simulation of channels of different aspect ratio. The dimensions of the simulated cases are (a) h = 225nm, w = 450nm, $\alpha = 1 < \alpha_1$, (c-d) h = 225nm, w = 270nm, $\alpha_1 < \alpha = 1.67 < \alpha_2$. Red circles denote the corner with bend deformation in (b), simulated without colloids, and splay deformation in (c), simulated with colloids. (e-f) h = 225nm, w = 135nm, $\alpha = 3.33 > \alpha_2$.

We found the minimum energy states by placing the colloid at various locations inside the channel, the energies of different states are first presented in simulation unit, the change in energy is presented in terms of k_BT. For channel dimension shown in Fig. 9(b-c), when the colloid is located in the middle of the cell, the total energy is U = -4541.64 (reference). As the colloid "moves" towards the corner, the energy decreases. When the colloid is located at the corner, but the corner has bend deformation as shown in Fig. 9(b), U = -4550.01, or lowered by $31k_BT$ from the reference; Finally, when the corner has splay deformation, the total energy is further lowered to U = -4555.98, lowered by $54k_BT$ from reference; For channel dimension shown in 9(d-e), we start by placing both colloids at a distance of 45nm away from all the walls and achieve a total energy U = -2630.52 (reference). As we move the colloid to closer and closer to corners, the energy steadily lowers, until it reaches a minimum of U = -2669.84, lowered an additional ΔU = $149k_BT$ when both colloids are located at the corners as shown in Fig. 9(e).

The difference of scale may lead to differences in the system behavior in numerics and experiments. Currently available computation power cannot fully resolve the fun-

damental difference in scale. In particular, given that our system's colloids are small (5μm) compared with the groove geometry dimensions ($\sim$100μm), it is not possible to simulate colloids with dipoles in detail. In this work, simulation was used to provide guidance to augment various experimental methods. There is another important ratio to consider, that of colloid radius d to the anchoring extrapolation length $\xi = K/W$ (K is the elastic constant and W is the anchoring strength). The ratio $d/\xi = 5$ in experiment and 20 in simulation, as the anchoring strength is scaled inversely to system size in simulation. Nevertheless, in our numerics, as in experiments, the colloids serve to stabilize defect lines. These configurations are consistent with the minimum energy states achieved in simulation in grooves with $\alpha > \alpha_1$. Configurations of the lowest energy state in simulation for all three geometries are shown in Fig. 9.

[1] M. Škarabot, M. Ravnik, S. Žumer, U. Tkalec, I. Poberaj, D. Babič, and I. Muševič, Phys. Rev. E **77**, 061706 (2008).
[2] I. Muševič, M. Škarabot, U. Tkalec, M. Ravnik, and S. Žumer, Science **313**, 954 (2006).
[3] C. Blanc, D. Coursault, and E. Lacaze, Liq. Cryst. Rev. **1**, 83 (2013).
[4] A. D. Dinsmore, J. C. Crocker, and A. G. Yodh, Curr. Op. Coll. Int. **3**, 5 (1998).
[5] O. D. Lavrentovich, Liq. Cryst. **24**, 117 (1998).
[6] E. M. Terentjev, Phys. Rev. E **51**, 1330 (1995).
[7] T. C. Lubensky, D. Pettey, N. Currier, and H. Stark, Phys. Rev. E **57**, 610 (1998).
[8] J. C. Loudet, P. Barois, P. Auroy, P. Keller, H. Richard, and P. Poulin, Langmuir **20**, 11336 (2004).
[9] I. Muševič, M. Škarabot, U. Tkalec, M. Ravnik, and S. Žumer, Science **313**, 954 (2006).
[10] J.-B. Fleury, D. Pires, and Y. Galerne, Phys. Rev. Lett. **103**, 267801 (2009).
[11] H. Agha, J.-B. Fleury, and Y. Galerne, Eur. Phys. J. E **35**, 82 (2012).
[12] H. Yoshida, K. Asakura, J. Fukuda, and M. Ozaki, Nat. Commun. **6** (2015), 10.1038/ncomms8180.
[13] T. Araki, F. Serra, and H. Tanaka, Soft Matter **9**, 8107 (2013).
[14] G. P. Crawford, D. W. Allender, and J. W. Doane, Phys. Rev. A **45**, 8693 (1992).
[15] M. Cavallaro, M. A. Gharbi, D. A. Beller, S. Čopar, Z. Shi, T. Baumgart, S. Yang, R. D. Kamien, and K. J. Stebe, Proc. Natl. Acad. Sci. **110**, 18804 (2013).
[16] A. del Campo and C. Greiner, J. Micromech. Microeng. **17**, R81 (2007).
[17] I. I. Smalyukh, S. V. Shiyanovskii, and O. D. Lavrentovich, Chem. Phys. Lett. **336**, 88 (2001).
[18] See Supplemental Material V1 at [URL] for an eyelash imaged in BF by moving the objective focus.
[19] M. Ravnik and S. Žumer, Liq. Cryst. **36**, 1201 (2009).
[20] D. A. Beller, M. A. Gharbi, and I. B. Liu, Soft Matter **11**, 1078 (2015).
[21] D. A. Beller, *Controlling Defects in Nematic and Smectic Liquid Crystals Through Boundary Geometry*, Ph.D. thesis, University of Pennsylvania, University of Pennsylvania (2014).
[22] A. Sengupta, C. Bahr, and S. Herminghaus, Soft Matter **9**, 7251 (2013).
[23] Y. Xia, F. Serra, R. D. Kamien, K. J. Stebe, and S. Yang, Proc. Natl. Acad. Sci. **112**, 15291 (2015).
[24] N. M. Silvestre, P. Patricio, and M. M. Telo da Gama, Phys. Rev. E **69**, 061402 (2004).
[25] Z. Eskandari, N. M. Silvestre, M. M. Telo da Gama, and M. R. Ejtehadi, Soft Matter **10**, 9681 (2014).
[26] P.-G. D. Gennes and J. Prost, *The Physics of Liquid Crystals* (Oxford University Press, 1993).
[27] M. Kléman, Rep. Prog. Phys. **52**, 555 (1989).
[28] P. Poulin, H. Stark, T. C. Lubensky, and D. A. Weitz, Science **275**, 1770 (1997).
[29] T. C. Halsey and W. Toor, Phys. Rev. Lett. **65**, 2820 (1990).
[30] See Supplemental Material V2 at [URL] for a video of a cell-spanning wire viewed by changing focal plane under the microscope.
[31] See Supplemental Material V3 at [URL] for a video of the tracked colloids moving inside the channel.
[32] O. D. Lavrentovich, Soft Matter **10**, 1264 (2014).
[33] M. A. Gharbi, M. Cavallaro Jr, G. Wu, D. A. Beller, R. D. Kamien, S. Yang, and K. J. Stebe, Liq. Cryst. **40**, 1619 (2013).
[34] M. L. Blow and M. M. Telo da Gama, J. Phys.: Condens. Matter **25**, 245103 (2013).
[35] N. M. Silvestre, Z. Eskandari, P. Patrício, J. M. Romero-Enrique, and M. M. Telo da Gama, Phys. Rev. E **86**, 011703 (2012).
[36] See Supplemental Material V4 [URL] for isotropic-nematic transition in a narrow channel.